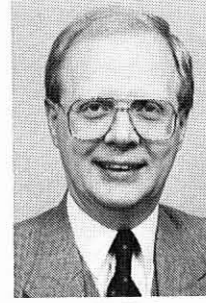


VABS: A New Concept for Composite Rotor Blade Cross-Sectional Modeling



Carlos E. S. Cesnik*
Post-Doctoral Fellow



Dewey H. Hodges
Professor

School of Aerospace Engineering
Georgia Institute of Technology
Atlanta, Georgia

A general framework for modeling composite rotor blades is presented. This framework extracts from a three-dimensional elasticity formulation two sets of analyses: one over the cross section, providing elastic constants that can be used in a suitable set of beam equations, and the other the beam equations themselves. The cross-sectional analysis, along with the accompanying engineering software (VABS), provides an accurate beam representation of the blade structure, allowing a designer to take advantage of composite materials when designing rotor blades. VABS is able to take into consideration anisotropic, nonhomogeneous materials and to represent general cross-sectional geometries, requiring neither the costly use of 3-D finite element discretization nor the loss of accuracy inherent in any simplified representation of the cross section. Results obtained from analysis of a variety of composite beams are presented. The generality of the method and accuracy of the results should increase confidence at the design stage that the structure will perform as expected and, consequently, should lower costs from experimental tests and further adjustments.

Introduction

Due to their geometries, rotor blades have one dimension that is much larger than the other two. Such flexible structures can often be treated as a beam, a one-dimensional (1-D) body. This idealization of the actual structure leads to a much simpler mathematical formulation than would be obtained if complete three-dimensional (3-D) elasticity were used to model it (see Fig. 1). To do so, one has to find a way to capture the behavior associated with the two dimensions that are being eliminated by correctly accounting for geometry and material distribution. The process that takes the original 3-D body and represents it as a 1-D one is called "dimensional reduction."

In this present work, finite-element-based nonhomogeneous anisotropic initially curved and twisted beam theory was formulated from geometric nonlinear, 3-D elasticity. The kinematics were derived for arbitrary warping (which includes out-of-plane as well as in-plane deformations) based upon the concept of decomposition of the rotation tensor. The 3-D strain energy based on this strain field is dimensionally reduced via the variational-asymptotical method (Ref. 1). The 3-D warping is calculated in terms of the 1-D strain measures and the functions in the strain energy become independent of the cross-sectional variables. The resulting equations govern both sectional and global deformation, as well as provide the 3-D displacement and strain fields in terms of beam deformation quantities. The formulation also naturally leads to geometrically exact, 1-D kinematical and intrinsic equilibrium equations for the beam deformation (Ref. 2).

The current theory provides a very general framework of modeling initially curved and twisted beams, allowing one to deal with different effects

without the use of ordering schemes or other *ad hoc* restrictions. This theory is not limited to the low-order theory found in classical approaches. Moreover, it is not limited to the usual Saint-Venant approach for the interior problem associated with beams. Rather, the asymptotical method allows for the approximation of the cross-sectional behavior in terms of the eigenfunctions of a certain Sturm-Liouville problem associated with the cross section. These eigenfunctions contain all the necessary information about the nonhomogeneities throughout the cross section of the beam and thus possess the appropriate discontinuities in the derivatives of displacement. The new "degrees of freedom" associated with these eigenfunctions for the beam cross section allow for treatment of transverse shear deformation and restrained warping in a systematic way (Ref. 8). The approach is based on the identification of small parameters in the structure, and the cross section may have arbitrary geometry (solid or thin-walled, closed or open). The idea is to be able to model a complex structure (*e.g.*, an actual airfoil-shaped cross section, with all its components and different materials) rather than a simplified version of it.

Fig. 2 represents the schematic of a unified process for analyzing composite beams and the shaded blocks represent the extension of the current work.

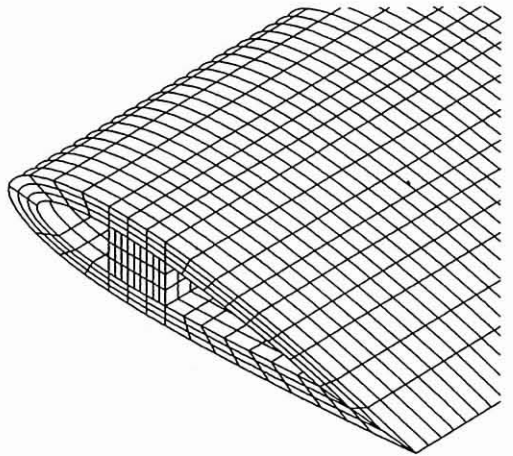
Cross-Sectional Analysis

In constructing a 1-D beam theory from 3-D elasticity, the strain energy stored in a 3-D body if represented by the strain energy which would be stored in an imaginary 1-D body. This modeling process *cannot* be performed in an *exact* manner. However, due to the interest of working with a simple 1-D theory, researchers have turned to asymptotical methods in order to reduce the dimension of the model for bodies which contain one or more small parameters.

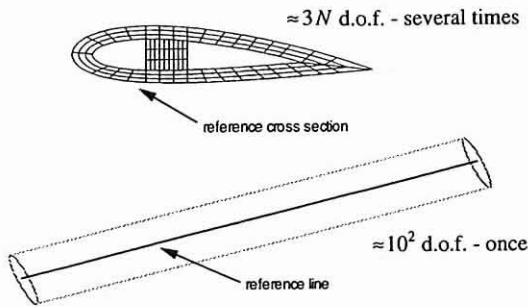
Thus, in what follows the 3-D beam problem is replaced by an *approximate* 1-D one in which the strain energy per unit length will be a function only of $x_1 \equiv x$ (length along a reference line r within an undeformed beam;

Presented at the American Helicopter Society 51st Annual Forum, Fort Worth, TX, May 9-11, 1995. Copyright ©1995 by the American Helicopter Society, Inc. All rights reserved. Manuscript received July 1995; accepted Sept. 1996.

*Presently Boeing Assistant Professor of Aeronautics and Astronautics, Massachusetts Institute of Technology, Cambridge, MA.



(a) 3-D discretization
($\approx 10^4 N$ d.o.f. — once)



(b) Two-step modeling process

Fig. 1. Schematic of the discretization process for a rotor blade structure (N = number of nodes in a cross section).

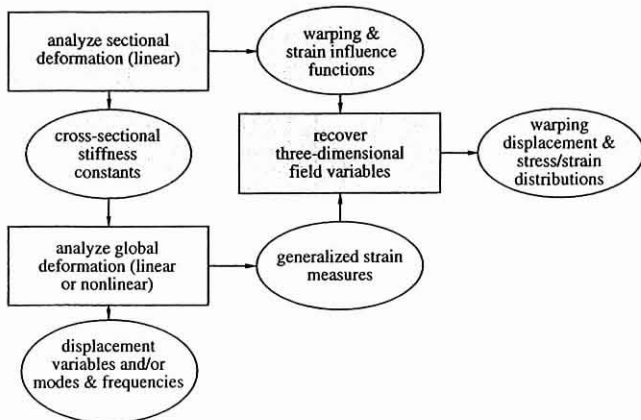


Fig. 2. Overview of beam analysis (shaded boxes represent the scope of the present work).

x_2 and x_3 denote lengths along lines orthogonal to the reference line r). This will be done with the aid of the variational-asymptotical formulation (Refs. 3,4). The kinematics of the beam are based on the general formulation of Danielson and Hodges (Ref. 5). Local rotation, as defined therein, is taken to be of the order of the strain. Since only geometrically nonlinear behavior is considered, the strain can be treated as small relative to unity

without imposing any explicit restrictions on the magnitudes of the displacement of the reference line or the section rotation. Subject only to these restrictions, all possible deformations of beams are taken into account in the analysis. The theoretical development is only outlined herein and more detail can be found in Refs. 6 and 5.

3-D Formulation

As described in Refs. 7 and 8, we first derive the 3-D formulation, the solution of which shall be considered the exact solution of the beam problem.

Strain Field. From the work of Danielson and Hodges (Ref. 5), under the condition of small local rotation, Jaumann strain components Γ^* (a 3×3 symmetric matrix) can be expressed by

$$\Gamma^* = \frac{1}{2} (\chi + \chi^T) - I \tag{1}$$

$$X_{mn} = \mathbf{B}_m \cdot \frac{\partial \hat{\mathbf{R}}}{\partial \chi_k} \mathbf{g}^k \cdot \mathbf{b}_n$$

where I is the 3×3 identity matrix, $\hat{\mathbf{R}}$ is the position vector which points to an arbitrary point in the deformed beam, \mathbf{g}^k is the contravariant base vector for the undeformed state, and \mathbf{B}_m and \mathbf{b}_n are components of the orthonormal reference triads in the deformed and undeformed states, respectively.

From the above equation, the strain field can be expressed as a 6×1 column matrix

$$\Gamma = [\Gamma_{11}^* \ 2\Gamma_{12}^* \ 2\Gamma_{13}^* \ \Gamma_{22}^* \ 2\Gamma_{23}^* \ \Gamma_{33}^*]^T$$

so that

$$\Gamma = \frac{1}{h} \Gamma_h v + \Gamma_\epsilon \epsilon + \Gamma_R v + \Gamma_\ell v' \tag{2}$$

where matrices Γ_h (6×3), Γ_ϵ (6×4), Γ_R (6×3) and Γ_ℓ (6×3) are

$$\Gamma_h = \begin{bmatrix} 0 & 0 & 0 \\ \frac{\partial}{\partial \zeta_2} & 0 & 0 \\ \frac{\partial}{\partial \zeta_3} & 0 & 0 \\ 0 & \frac{\partial}{\partial \zeta_2} & 0 \\ 0 & \frac{\partial}{\partial \zeta_3} & \frac{\partial}{\partial \zeta_2} \\ 0 & 0 & \frac{\partial}{\partial \zeta_3} \end{bmatrix}$$

$$\Gamma_\epsilon = \frac{1}{\sqrt{g}} \begin{bmatrix} 1 & 0 & -\zeta_3 & \zeta_2 \\ 0 & \zeta_3 & 0 & 0 \\ 0 & -\zeta_2 & 0 & 0 \\ 0 & 0 & 0 & 0 \\ 0 & 0 & 0 & 0 \\ 0 & 0 & 0 & 0 \end{bmatrix} \tag{3}$$

$$\Gamma_R = \frac{1}{\sqrt{g}} \left[\tilde{k} + k_1 I \begin{pmatrix} \zeta_3 \frac{\partial}{\partial \zeta_2} & -\zeta_2 \frac{\partial}{\partial \zeta_3} \\ 0 & 0 \end{pmatrix} \right]$$

$$\Gamma_\ell = \frac{1}{\sqrt{g}} \begin{bmatrix} I \\ 0 \end{bmatrix}$$

Here $\tilde{\gamma}_{nm} = -e_{nmk}(\cdot)_k$, and the column matrix ϵ represents the 1-D measures of deformation

$$\epsilon = \left\{ \begin{matrix} \gamma \\ h\kappa \end{matrix} \right\} \tag{4}$$

where γ is the average cross-sectional extensional strain (the axial force strain measure) defined as

$$\gamma = \mathbf{R}' \cdot \mathbf{B} - 1 \tag{5}$$

and column matrix $\kappa = [\kappa_1 \ \kappa_2 \ \kappa_3]^T$ contains the so-called moment strain measures

$$\kappa_n = K_n - k_n \tag{6}$$

and k is the initial curvature vector, the elements of which are the pretwist k_1 , and the initial curvatures k_2 and k_3 . The 3-D warping is denoted by v . The metric determinant g can be calculated as

$$\sqrt{g} = 1 - x_2 k_3 + x_3 k_2 \tag{7}$$

where x_2 and x_3 are cross-sectional local Cartesian coordinates which vary in the prescribed domain S . The characteristic size of the domain S is denoted by h and the dimensionless coordinates $\zeta \equiv \{\zeta_2 \equiv x_2/h, \zeta_3 \equiv x_3/h\}$ are introduced.

The small parameter ϵ can be now specified as

$$\epsilon = \max\|\epsilon\| \tag{8}$$

A few nonlinear terms in the strain field, which couple v and ϵ , have been neglected in Eq. (2) because a physically linear beam theory is to be developed. The form of the strain field is of great importance because it now linear in ϵ , v and its derivatives. This is the only point where ϵ as a small parameter needs to be taken into account.

Strain Energy of a Beam. The strain density for a beam per unit length can be written as

$$U = \frac{1}{2} \langle \Gamma^T D \Gamma \rangle \tag{9}$$

where D is the 6×6 symmetric material matrix in the \mathbf{b}_n basis and the notation

$$\langle \bullet \rangle = \int_S \bullet \sqrt{g} dx_2 dx_3 = h^2 \int \bullet \sqrt{g} d\zeta_2 d\zeta_3 \tag{10}$$

is used throughout the paper.

The 3-D Jaumann stress Z , which is conjugate to the Jaumann strain Γ is

$$Z = D\Gamma \tag{11}$$

Small Parameters

There are four characteristic parameters in the considered theory, two of which, h and ϵ , have already been introduced. Two others are the characteristic length ℓ , over which the deformation state varies in the longitudinal direction, and the characteristic length of the initial curvature and twist $R = 1/\sqrt{k_1^2 + k_2^2 + k_3^2}$. Thus, for a pretwisted straight beam, $R = 1/k_1$, and for a non-pretwisted beam curved about x_α , $R = 1/k_\alpha$, where $\alpha = 2, 3$. We will expand the warping $v_n(x, \zeta)$ as a series with respect to the small parameters $\frac{h}{\ell}$ and $\frac{h}{R}$. Since both of them have the same numerator, expansion in $\frac{h}{\ell}$ and $\frac{h}{R}$ is the same as the expansion in h only.

We will therefore consider h to be the only small parameter in spite of its dimension.

Discretization

The problem may be solved numerically by discretizing it with respect to the cross-sectional coordinates ζ_α . Considering the finite element discretization, the unknown functions $v_n(x, \zeta)$ can be represented as the product of a shape functions matrix $S(\zeta)$ and a column matrix of nodal values of $v(x, \zeta)$, denoted as $V(x)$

$$v(x, \zeta) = S(\zeta)V(x) \tag{12}$$

Substituting the above discretized unknown function into Eq. (9) and also taking into account Eq. (2), one obtains

$$2U = \left(\frac{1}{h}\right)^2 V^T E V + \left(\frac{1}{h}\right) 2V^T (D_{h\epsilon}\epsilon + D_{hR}V + D_{h\ell}V') + (1) (\epsilon^T D_{\epsilon\epsilon}\epsilon + V^T D_{RR}V + V'^T D_{\ell\ell}V' + 2V^T D_{R\epsilon}\epsilon + 2V'^T D_{\ell\epsilon}\epsilon + 2V^T D_{R\ell}V') \tag{13}$$

in which the following definitions were introduced

$$\begin{aligned} E &\triangleq \langle [\Gamma_h S] D [\Gamma_h S] \rangle & D_{\epsilon\epsilon} &\triangleq \langle [\Gamma_\epsilon]^T D [\Gamma_\epsilon] \rangle \\ D_{h\epsilon} &\triangleq \langle [\Gamma_h S] D [\Gamma_\epsilon] \rangle & D_{hR} &\triangleq \langle [\Gamma_h S] D [\Gamma_R S] \rangle \\ D_{h\ell} &\triangleq \langle [\Gamma_h S] D [\Gamma_\ell S] \rangle & D_{R\epsilon} &\triangleq \langle [\Gamma_R S] D [\Gamma_\epsilon] \rangle \\ D_{\ell\epsilon} &\triangleq \langle [\Gamma_\ell S] D [\Gamma_\epsilon] \rangle & D_{RR} &\triangleq \langle [\Gamma_R S] D [\Gamma_R S] \rangle \\ D_{R\ell} &\triangleq \langle [\Gamma_R S] D [\Gamma_\ell S] \rangle & D_{\ell\ell} &\triangleq \langle [\Gamma_\ell S] D [\Gamma_\ell S] \rangle \end{aligned} \tag{14}$$

Modal Approximation

The strain energy is shown in Eq. (13) in its most general form. From here on, each specific formulation is derived depending on how we consider the displacement field component V . For example, if V is the small perturbation in the classical displacement field (three translations and the rotation about the beam axis), then it only contains the original definition of the 3-D warping field. But in order to make the beam functional more flexible with respect to the variable x , consider the introduction of new unknown beam functions such that

$$V(x) = \Psi_q q(x) + W(x) \tag{15}$$

where q is a column matrix of one or more new unknown functions, and Ψ_q is a matrix, of which each column represents a ζ -mode shape associated with one of the new unknown functions $q(x)$. These are denoted as the "new degrees of freedom." The new warping to be found now is W .

Various Stiffness Models

As discussed above, depending on the choice of Ψ_q , different stiffness matrices are derived. By defining the stiffness matrix by A with the appropriated subindex, the different results may be summarized as follows:

"Classical" 4 x 4 Stiffness Matrix. The "Classical" 4×4 stiffness matrix, with measures of extension, twist, and bending.

$$2U = \epsilon^T A_{cl} \epsilon \tag{16}$$

Even though "classical" in form, it goes well beyond Euler-Bernoulli theory in rigor, and the nonclassical material coupling effects (bending-shear and extension-shear couplings) are correctly accounted for.

"Timoshenko-like" 6 x 6 Stiffness Matrix. Beside the four classical measures, this formulation explicitly includes transverse shear deformations at the kinematical level.

$$2U = \begin{pmatrix} \gamma_{11} \\ 2\gamma_{12} \\ 2\gamma_{13} \\ K_1 \\ K_2 \\ K_3 \end{pmatrix}^T [A_T] \begin{pmatrix} \gamma_{11} \\ 2\gamma_{12} \\ 2\gamma_{13} \\ K_1 \\ K_2 \\ K_3 \end{pmatrix} \tag{17}$$

This can be seen as the first attempt to include higher-order effects in the classical theory, creating a Timoshenko-like theory. Another way to handle this problem in an asymptotically consistent way is addressed in Ref. 9 for the plate problem and could be adapted for this problem as well.

“Extended” $(4 + 2N_q) \times (4 + 2N_q)$ Stiffness Matrix. A general way to include higher-order effects in the classical theory is presented by introducing N_q new unknown beam functions, represented by ζ -mode shapes Ψ_q (cross-section dependent) and corresponding “new degrees of freedom” $q(x)$.

$$2U = \left\{ \begin{matrix} \epsilon \\ \frac{1}{h}q \\ q,x \end{matrix} \right\}^T \begin{bmatrix} A_{\epsilon\epsilon} & A_{\epsilon q} & A_{\epsilon\ell} \\ A_{q\epsilon} & A_{qq} & A_{q\ell} \\ A_{\ell\epsilon} & A_{\ell q} & A_{\ell\ell} \end{bmatrix} \left\{ \begin{matrix} \epsilon \\ \frac{1}{h}q \\ q,x \end{matrix} \right\} \quad (18)$$

In this general situation, Ψ_q can be evaluated from an eigenvalue problem (Ref. 6) or from direct selection by the engineer. A simple case is the Timoshenko-like theory, the stiffnesses of which could be computed by incorporating two Ψ_q as rigid-body rotations of the reference cross section about x_2 and x_3 . The incorporation of such “non-classical” cross-sectional degrees of freedom is also quite useful when analyzing open-section beams, for which explicit restraint of these quantities is necessary. At present one must take into consideration short-wavelength extrapolation to ensure a correct stiffness model (Ref. 8). (A more “engineering-oriented” approach to this problem is currently under development by the authors.)

The full expressions for these various stiffness matrices described above can be found in Ref. 6 or, for example, in Refs. 8 and 10.

1-D Formulation

The non-linear one-dimensional equations for the 4×4 as well as 6×6 stiffness matrices can be found in Ref. 2. If one considers the new degrees of freedom q is the beam analysis derivation, a new set of equilibrium equations is added to the one derived in Ref. 2. This new set of equations is decoupled from the other equilibrium equations (the coupling appears only at the constitutive equation level) and can be summarized as

$$\begin{aligned} F' + \tilde{K}F + f &= 0 \\ M' + \tilde{K}M + (1 + \gamma_{11})\tilde{e}_1F + m &= 0 \\ P' - Q + f_q - (f_q) &= 0 \end{aligned} \quad (19)$$

where F is a column matrix corresponding to three beam forces (axial, shear along x_2 , and shear along x_3) and M to three moments (torsional, bending about x_2 , and bending about x_3), all expressed in the \mathbf{B}_i basis. f and m are column matrices containing the applied force per unit length and moment per unit length, respectively. The new degrees of freedom q 's introduce corresponding generalized forces Q and P , and the measures f_q and f_q are distributed generalized loads associated with Q and P respectively.

The kinematical equations that go along with the rest of the 1-D problem are

$$\begin{aligned} \gamma_{11} &= e_1^T C (e_1 + u' + \tilde{k}u) - 1 \\ e_\alpha^T C (e_1 + u' + \tilde{k}u) &= 0 \\ K &= \kappa + k \quad \tilde{\kappa} = -C' C^T + C \tilde{k} C^T - \tilde{k} \end{aligned} \quad (20)$$

where u is a column matrix containing the three displacements in the \mathbf{b}_i basis, and the global rotation matrix

$$C = \frac{\left(1 - \frac{\theta^T \theta}{4}\right) I - \tilde{\theta} + \frac{\theta \theta^T}{2}}{1 + \frac{\theta^T \theta}{4}} \quad (21)$$

given in terms of the Rodrigues parameters θ . A detailed description of the 1-D formulation, including the dynamic behavior, can be found in Ref. 2 and the implementation in Ref. 11, for example.

Implementation of the Theory

The developed theory was implemented numerically in a finite-element computer code call **VABS** (*Variational-Asymptotical Beam Sectional Analysis*). From it one can get the stiffness constants and warping field over the cross section. Along with 1-D codes (e.g., Ref. 12), beam results are generated and the 3-D stress/strain distribution can be recovered.

Finite Element Formulation

As shown before, in order to eliminate the warping (v) from the energy density (Eq. 9), one has to turn to a numerical solution. The finite element formulation is the natural choice for this kind of problem, where arbitrary geometry and material distribution are present in the domain of the problem.

Since the domain must be homogeneous at the element level, elements are not allowed to cross a lamina boundary. Also, due to the manufacturing process used in laminated composite structures, the planar quadrilateral element is the recommended choice. There were three types of elements generated to deal with the cross-section discretization:

- (a) 4-node rectangular element
- (b) 6-node isoparametric element
- (c) 8-node isoparametric element

and they are represented in Fig. 3. Shape functions for a planar quadrilateral element are the standard one given in Ref. 13, for example.

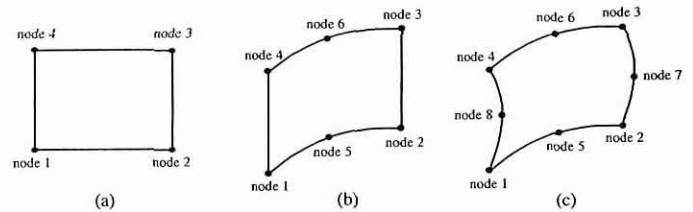


Fig. 3 (a) Four-node rectangular element; (b) Six-node isoparametric element; (c) Eight-node isoparametric element.

Among the above elements, the 4-node rectangular element has the main advantage of being simple. But for most of the practical applications, the cross section has one or more curved boundaries and a higher-order interpolation is necessary. So, quadratic interpolation was used on each side of the element along with the isoparametric formulation, providing a way to model curved boundaries. That leads to the 8-node isoparametric element. But due to the fact that usually no more than two nodes are necessary to discretize a typical pre-preg lamina through its thickness, the 6-node isoparametric element is the most efficient one. All the elements present three degrees of freedom per node, corresponding to the 3-D warping field.

Computer Code

VABS is the result of the theoretical formulation presented herein. From it one gets an asymptotically correct stiffness matrix and warping influence matrix for a general, nonhomogeneous, anisotropic beam cross section.

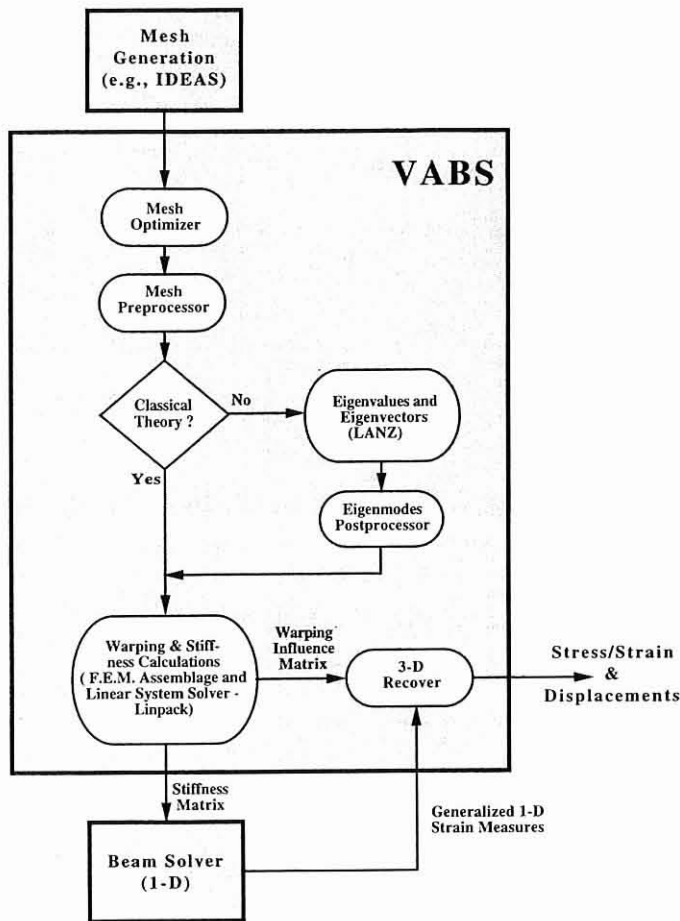


Fig. 4: VABS main blocks for stiffness calculation.

As shown in Fig. 4, VABS is divided in three main blocks:

- (a) Mesh preparation
- (b) Eigensystem solution
- (c) Warping and Stiffness calculations

Mesh preparation. The discretization of the cross-sectional domain is made by using one of the elements available for VABS. Even though VABS has a mesh generator developed for simple geometries, the user is supposed to provide the mesh input data.

Two filters to convert the Universal File format generated by CAD software, such as I-DEAS (Ref. 14), to standard input of VABS were created. They are able to deal with 6-node and 8-node elements. Also, an automatic nodal renumbering routine is available at the point in the procedure where the input data is prepared. It is used to reduce the bandwidth of the matrices involved in the problem by optimizing the enumeration of the nodes in the model and is a direct implementation of Ref. 15. An even more attractive option is to use the standard NASTRAN (Ref. 16) bulk data format. The mesh can be again generated by any compatible CAD package, and converted to VABS input format by NASVABS (Ref. 17) (a NASTRAN-to-VABS interface) before sending it to stiffness calculations.

Finally, a customized mesh preprocessor is available to the user in order to check the modeled geometry and material distribution of the problem. Again, since the input mesh can be given in NASTRAN bulk data format, several commercial packages may be used for that as well.

Eigensystem solution. In order to use the “new degrees of freedom” approach, an eigenproblem might need to be solved before the actual stiffness calculations start. This is going to provide the eigenvectors and eigen-

values other than the classical ones (i.e., zero eigenvalue with multiplicity four and the corresponding eigenvectors) of the generalized eigensystem. The selection of the important modes is based on a certain “influence coefficient matrix” described in detail in Ref. 6. So, one deals with large sparse matrices, and only the first N_q eigen-pairs are of some interest, where N_q is much smaller than the dimension of the matrices involved in the problem. Therefore, a suitable algorithm should be used to take advantage of those characteristics. Several methods for solving this problem exist. The choice was for the Lanczos’s method (Ref. 18), originally applied to solve large, sparse, symmetric eigenproblems. An algorithm based on this method for a generalized eigenproblem was numerically implemented in a computer package called LANZ (Ref. 19). In Ref. 20, it was shown that the Lanczos method is superior to the well-known subspace iteration (Ref. 13) in a sequential machine. Jones and Patrick (Ref. 21) showed that LANZ’s margin of superiority over subspace iteration is even greater in a vectorized machine.

Again, a postprocessor is provided to visualize the deformed mesh for a given eigenvector and compare it to the undeformed one.

Warping and stiffness calculations. The core of VABS is the warping and stiffness calculations. To obtain the warping influence matrix, a linear system of equations with several right-hand side vectors is solved. The stiffness calculation is divided in submatrices, e.g., the ones described in Eq. (18). This division is basically designed to avoid unnecessary calculations when there are only classical degrees of freedom and/or when the beam is prismatic. Two output files are generated, one for report purposes and the other one to be sent to the 1-D analysis.

Finally, after the beam analysis has been performed, the 1-D measures are fed back to VABSTR (Ref. 17) and the strain/stress fields are calculated within each element of the given cross section. A postprocessor is available to visualize the fields.

Numerical Results

For several different cross-sectional shapes and material distributions, beam geometries (including initial twist and curvature), and loading conditions, results from the current work were compared with experimental, analytical and other numerical results whenever available. Extensive validation of the code was done based on isotropic beams, where analytical and/or experimental results are available, and those are omitted from the present paper. In what follows, VABS is used to analyze several composite beams in order to demonstrate its versatility. Since some of the beam configurations have already been presented in earlier papers, details of them can be found in the indicated reference.

Rectangular Blade (BT) and (ET)

Consider two composite beams studied both experimentally and theoretically by Minguet and Dugundji (Ref. 22) with the following layups

$$\begin{aligned}
 \text{(BT):} & \quad [45^\circ / 0^\circ]_{3s} \\
 \text{(ET):} & \quad [20^\circ / -70^\circ / -70^\circ / 20^\circ]_{2a}
 \end{aligned}$$

Where BT reflects the fact that the prismatic beam has bending-twist coupling and ET that the prismatic beam has extension-twist coupling. The beams have thin rectangular cross sections of width 1.182 in and of thickness 0.05792 in and 0.07565 in, respectively. The beams are 22.05 in long and is vertically loaded 21.67 in from the root. The material used is the AS4/3501-6 Graphite/Epoxy, the properties of which and other details can be found in Ref. 4.

In Fig. 5, the displacements (far in the non-linear range) of the symmetric laminate BT are shown as a function of the magnitude of the verti-

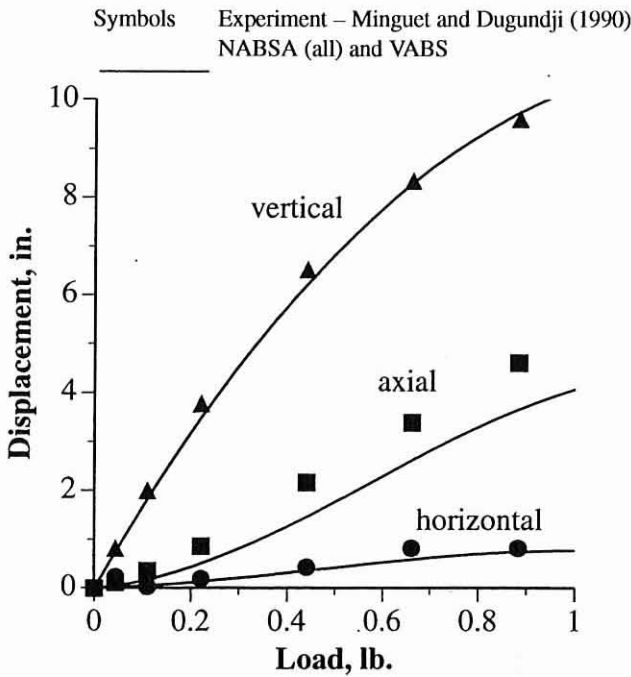


Fig. 5: Displacements of symmetric beam (BT).

cal load. As an independent numerical comparison, we use the results obtained from NABSA (Ref. 23), a finite element code based on the virtual work principle, and also the corresponding condensation of the 6×6 stiffness matrix by minimizing the energy with respect to the transverse shear measures (e.g., see Ref. 4). The theoretical results from all the stiffness models, including the full NABSA 6×6 , the reduced NABSA 4×4 , NABSA with transverse shear deformation set equal to zero (Euler beam theory), and the present result from the classical part of VABS, all show as one curve to within plotting accuracy, and agree with the experimental data very well. This is not too surprising since in this case the reduction operation only slightly changes the axial stiffness (because of extension-shear coupling). Studying only these results, one might (falsely, as shown below) conclude that transverse shear deformation could be set equal to zero at the outset and not hamper the predictive capability of the model.

In Fig. 6, the displacements of the beam with the antisymmetric laminate (ET) are shown. The dashed lines are the Euler-beam results (Incorrect "Classical") obtained by setting shear deformation equal to zero in the strain energy based on the full 6×6 stiffness matrix. These results are clearly inferior because the model is considerably stiffer than it should be. However, the theoretical results from the other three stiffness models, including the full NABSA 6×6 , the reduced NABSA 4×4 , and the present result from VABS (these last two being in the correct "Classical" form), all show as one curve to within plotting accuracy. This shows that for this case the 4×4 stiffness model is sufficient for predicting the same behavior as the 6×6 model.

Box Beam (B1)

A box beam case was taken from Stemple and Lee (Ref. 24) and has the following stacking sequence

$$(B1): [20^\circ / -70^\circ / 20^\circ / -70^\circ / -70^\circ / 20^\circ]_T$$

The corresponding geometric properties are shown in Fig. 7. The material is the T300/5208 Graphite/Epoxy and its properties can be found in Ref. 8.

This case presents a circumferentially uniform stiffness (CUS) configuration which produces extension-twist coupling. The cross section was discretized with 360 eight-node isoparametric elements for a total of 1200

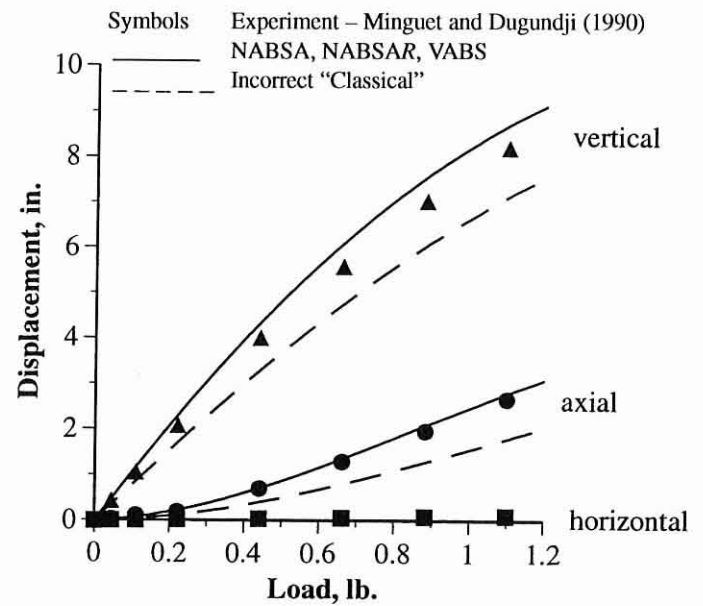


Fig. 6: Displacements of antisymmetric beam (ET).

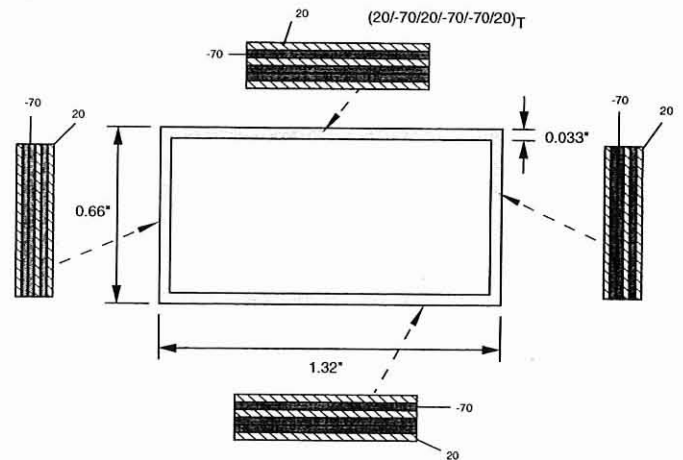


Fig. 7: Box Beam (B1) cross section geometry and material.

nodes and 3600 degrees of freedom.

This box beam configuration was also studied by Hodges *et al.* (Ref. 25) and Berdichevsky *et al.* (Ref. 26). Table 1 shows the flexibility results from the present classical theory in comparison with NABSA (Ref. 26), and TAIL (Ref. 27) results. The flexibility coefficients F_{ij} were obtained by inverting the stiffness matrix and the numbers in parenthesis correspond to the difference between that coefficient and the result obtained from NABSA (used as a reference).

As one can see, the classical theory coincides very closely with the corresponding NABSA results. Even though Ref. 26 is asymptotically correct to the same order as the present "Classical" Theory, the inclusion of an additional small parameter, i.e., the thickness of the cross-sectional wall, apparently eliminated terms that should be preserved due to material distribution.

Box Beam (B2)

A second box beam case was chosen among the experimental studies presented in Ref. 28.

$$(B2): [45^\circ]_6$$

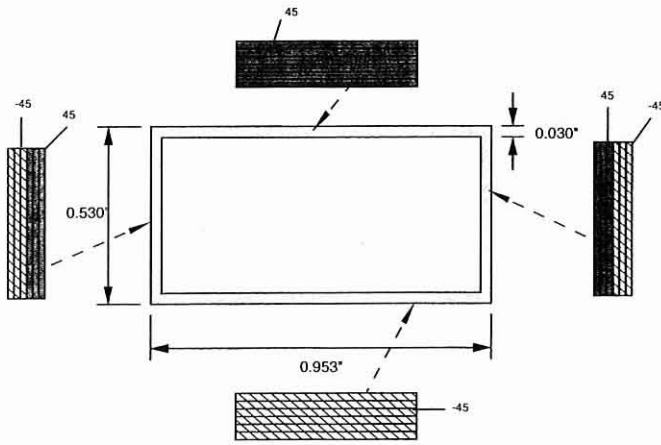


Fig. 8: Box Beam (B2) cross section geometry and material.

The corresponding geometric properties are shown in Fig. 8. The material properties are based on the AS4/3501-6 Graphite/Epoxy (see Ref. 6).

This case presents a circumferentially asymmetric stiffness (CAS) configuration which produces bending-twist coupling. It is also known by the name symmetric configuration as adopted by Chandra *et al.* (Ref. 28) and Smith and Chopra (Ref. 29).

The cross section was discretized with 540 six-node isoparametric elements for a total of 1260 nodes and 3780 degrees of freedom.

Table 1: Flexibility results for the Box Beam (B1) (1 extension; 2 torsion; 3, 4 bending)

Flexibility	NABSA	Ref. 26	TAIL	VABS
$F_{11} \times 10^6$	1.439	1.449 (+0.7%)	1.449(+0.7%)	1.431(-0.5%)
$F_{12} \times 10^6$	-4.178	-4.301 (+2.9%)	-4.301(+2.9%)	-4.225(+1.1%)
$F_{22} \times 10^5$	3.121	3.236 (+3.6%)	3.236(+3.6%)	3.172(+1.6%)
$F_{33} \times 10^5$	1.837	1.886 (+2.6%)	1.729(+5.8%)	1.837(+0.0%)
$F_{44} \times 10^5$	6.143	6.345(+3.2%)	5.016(+18.4%)	6.194(+0.8%)

In Fig. 9, the induced twist angle of a cantilever beam due to a unit vertical tip load is plotted against the spanwise coordinate. The present approach is put together with the experimental result and with the analytical predictions of Berdichevsky *et al.* (Ref. 26), Rehfield and Atilgan (Ref. 30), and Smith and Chopra (Ref. 29). As one can see, the correlation of the present approach with the experimental results is quite good. Even though Ref. 26 is based on a similar asymptotical approach, the thickness effect apparently prevents it from yielding better agreement with the experimental results. The complete thickness effect is included in the present numerical formulation. The inclusion of new degrees of freedom does not change this solution within plotting accuracy.

I-Beam (IB)

For the open-section configuration, a particular case from the experimental study done by Chandra and Chopra (Ref. 31) was chosen. It is a bending-twist-coupled cantilever I-beam. The cross section is made with graphite/epoxy material and Fig. 10 shows the geometric configuration. The cross section was discretized using 590 6-node isoparametric elements for a total of 1277 nodes and 3931 degrees of freedom.

One can take only the most dominant mode associated with torsion from the eigenanalysis. The "coefficient of influence" indicates that mode 11 is the most dominant one. It is reproduced in Fig. 11. The mode matches what was expected from the engineering theory like Ref. 32.

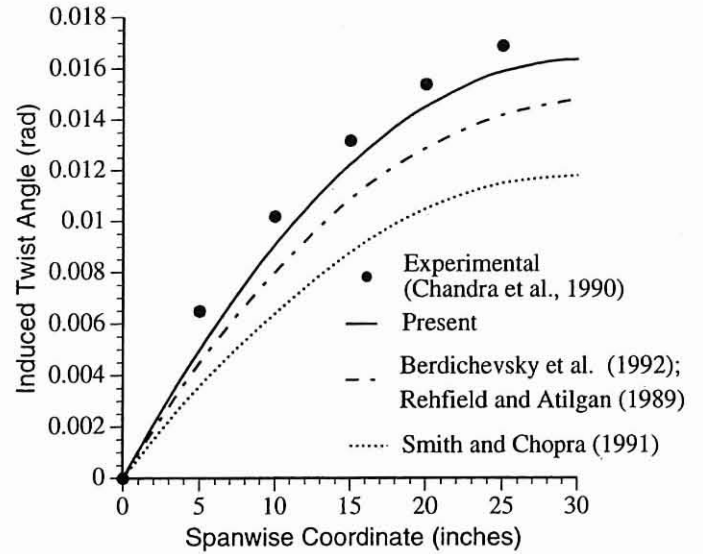


Fig. 9: Induced twist distribution along the beam length for the box beam (B2) due to a unit vertical tip load.

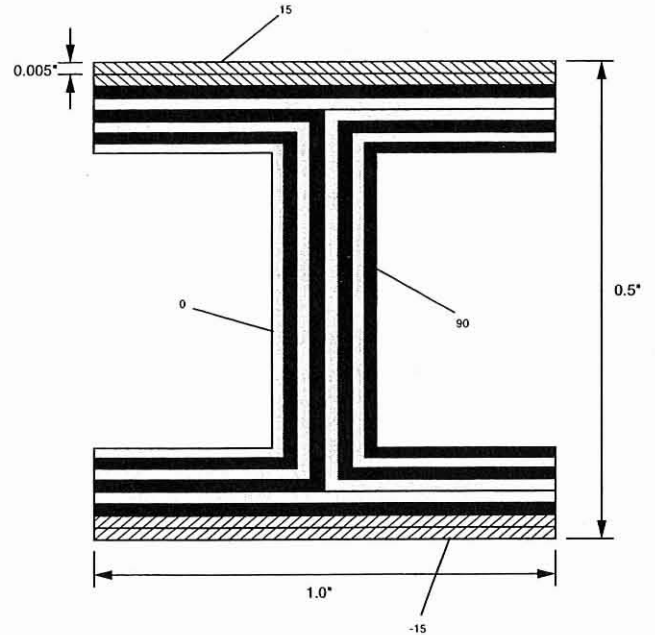


Fig. 10: I-Beam cross section geometry and material.

Therefore, considering only one extra degree of freedom q , one obtains a 6×6 stiffness matrix. This result has to go to a certain short wavelength extrapolation and the details of it is presented in Ref. 6. With the corrected stiffness matrix, the present theory predicts a behavior which is in good agreement with the experimental results from Ref. 31 (see Fig. 12). The other solutions shown on Fig. 12 are from Badir *et al.*, (Ref. 33) which also uses the variational-asymptotical approach, and from Chandra and Chopra (Ref. 31). As expected, the reduced 4×4 stiffness matrix ("Classical" theory) is unable to reproduce such behavior, introducing up to 100% error in the prediction of the induced twist angle at the tip.

Variable Angle-Ply Laminates (APs) and (APa)

To study some of the effects of initial twist and curvature in the stiffness constants of a beam, consider a thin rectangular cross section with dimensions 26.8 mm by 2.68 mm. (We note that h here is the larger dimen-

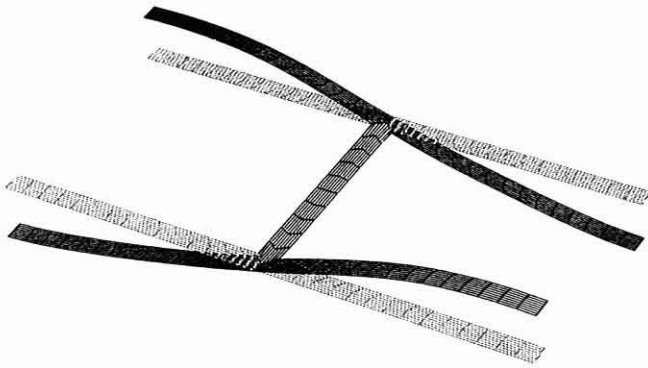


Fig. 11: Non-Classical Mode 11 for the composite I-Beam (IB).

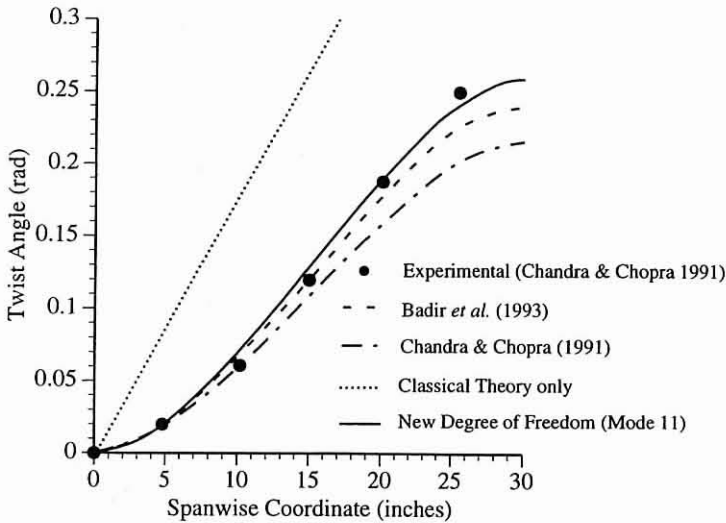


Fig.12. Twist distribution along the beam length for the I-Beam (IB) due to a unit tip torsional load.

sion 26.8 mm.) Two layups were studied, following Ref. 34, and both were discretized using a 12 x 20 6-node-element mesh (with quadratic interpolation across the width). They are defined as:

(APs): $[\theta / -\theta]_s$
 (APa): $[\theta_2 / -\theta_2]$

where the first is a symmetric layup with bending-twist coupling and the second is an antisymmetric configuration which presents extension-twist coupling. The material used is T300/5208 Graphite/Epoxy (Ref. 34). The cross-sectional dimension used to non-dimensionalized the curvature measure is the width of the blade, thus $h = 26.8$ mm.

Blades with Initial Twist.

Few results are available in the literature for highly pretwisted composite beams. Here, we compare VABS results with the numerical results of Kosmatka (Ref. 34) for pretwisted beam stiffness and flexibility constants. This seems to be a very consistent approach, even though there is no way at this point to assess its level of asymptotical correctness. Non-dimensionalized cross-sectional constants were used in order to set a common

basis for comparison. The following definitions are used:

$$\text{Torsional Rigidity Ratio} = \frac{F_{cl(2,2)}^0}{F_{cl(2,2)}^{rr}}$$

$$\text{Torsional Stiffness Ratio} = \frac{A_{cl(2,2)}^{rr}}{A_{cl(2,2)}^0}$$

$$\text{Axial Rigidity Ratio} = \frac{F_{cl(1,1)}^0}{F_{cl(1,1)}^{rr}}$$

$$\text{Bending Rigidity Ratio} = \frac{F_{cl(3,3)}^0}{F_{cl(3,3)}^{rr}} \text{ or } \frac{F_{cl(4,4)}^0}{F_{cl(4,4)}^{rr}}$$

$$\text{Extension-Bending Stiffness Ratio} = \frac{A_{cl(1,4)}^{rr}}{A_{cl(4,4)}^0 h}$$

$$\text{Twist/Extension Ratio} = \frac{F_{cl(1,2)}^{rr}}{F_{cl(1,1)}^{rr}}$$

where $F_{cl}^0 = (A_{cl}^0)^{-1}$ is the flexibility matrix for a prismatic unidirectional ($\theta = 0^\circ$) thin strip, and $A_{cl}^{rr} = (F_{cl}^{rr})^{-1}$ is the stiffness matrix including quadratic corrections on the small parameter $\frac{h}{R} (= hk_1)$ when initial curvature is zero, thus symbolically representing the effect of initial twist.

Figs. 13 and 14 describe cross-sectional constants related to the antisymmetric layup and Figs. 15 and 16 to the symmetric layup, each with respect to the ply angle (θ) and the level of non-dimensional pretwist ($hk_1 \equiv \frac{h}{R}$). In these plots, the symbols represent the results from Ref. 34 (abbreviated by "K") and the present results by lines (VABS). As one can see, the basic trends are the same between the two numerical methods, indicating that significant changes in the stiffness constants are introduced by applying an initial twist on the rotor, an issue of great importance mainly for tilt-rotor design. Figs. 13 and 15 show a discrepancy between VABS results and the ones from Ref. 34 for high levels of pretwist. At the highest level of pretwist shown, $\frac{h}{R} = hk_1 = 0.3$, the maximum difference between the two numerical approaches is of the order of 10%. Based on independent analysis* we have concluded that the VABS results are closer to the exact solution than are those of the theory of Ref. 34 for the highest levels of pretwist presented herein. However, this is an issue that should be further addressed in light of experimental results and additional analytical research.

Blades with Initial Curvature.

A preliminary study of the influence of initial curvature in the stiffness constants of a composite blade was also done. The initial curvature (again non-dimensionalized by h , leading to $hk_3 \equiv \frac{h}{R}$) was taken about x_3 direction, so that $k_3 \geq 0$. For this case we have no other available result for comparison.

Fig. 17 shows the variation of the extension-bending stiffness constants for the APs configuration (the APa configuration shows similar trends (Ref. 35)). The maximum values of the coupling terms occur for $\theta \approx \pm 15^\circ$. The effects of the symmetric or antisymmetric layups are not significant for the general behavior. This is also the case for all the other constants. In fact, the effective axial rigidity as well as the effective bending rigidity ($F_{cl}^{rr}(3,3)$) are insensitive for the variation of k_3 . Both effective torsional rigidity and the other effective bending rigidity ($F_{cl}^{rr}(4,4)$) present similar

*The authors thank Mr. Dineshkumar Harursampath for providing results from his unpublished analysis, based on arbitrarily large twist for an anisotropic strip-like beam.

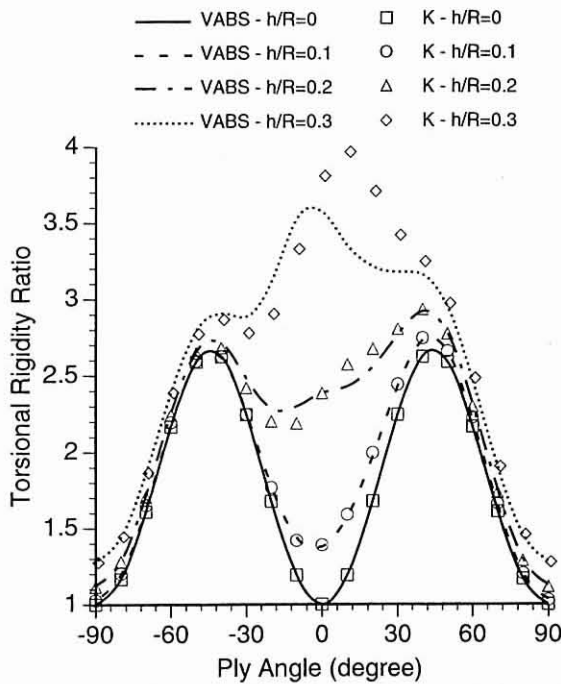


Fig. 13. Torsional rigidity ratio of APa for different levels of initial twist.

results, with the difference that there is an influence of initial curvature of up to 10% localized around $\theta = \pm 45^\circ$ and $\theta = 0^\circ$, respectively.

Rotor Blade (RB)

As one can see from the above results, VABS is well suited for evaluation of stiffness constants for a given cross section. In the following, the code provides stiffness results for an airfoil-shaped blade. This is done by modeling all the different components of the cross-sectional geometry and the different materials present in each of them. At this point, there is no need for simplification of the airfoil external geometry or its interior substructure, as often done by simple theories (the actual blade is far from having a box-beam shape or any other simplified geometry.) The way VABS is conceived, the form of the cross section is immaterial, and the asymptotical stiffness constants are evaluated within the same accuracy as the simplified ones showed before. Unfortunately, actual rotor blade data are not extensively available in the literature, so we present results for a simulated blade section, based on the geometric configuration described in Ref. 17.

Fig. 18 shows the blade geometry. As indicated there, four different materials were used which exemplify a typical material distribution for a rotor blade. The cross section was discretized by using 412 6-node elements with a total of 3915 warping degrees of freedom. VABS takes approximately 2.5 minutes of CPU time in an HP9000/735 machine in order to do this cross-sectional analysis once.

Any of the analyses previously presented can be similarly done for this rotor blade. Fig. 19 shows the appearance of extension-twist coupling due to initial twist and its consequence in the axial rigidity ratio, Fig. 20; the torsional rigidity and torsional stiffness ratios, Fig. 21; and finally in the bending rigidities ratios, Fig. 22.

The modes and frequencies, as well as aeroelastic stability, could be calculated in the same way they are done, for example, in Refs. 11 and 12. 3-D stress/strain recovery is also possible, and a few such cases are discussed in Ref. 17, including the same rotor blade geometric configuration. This provides the rotor designer with great flexibility in exploring different design options with the actual rotor blade configuration using a high-

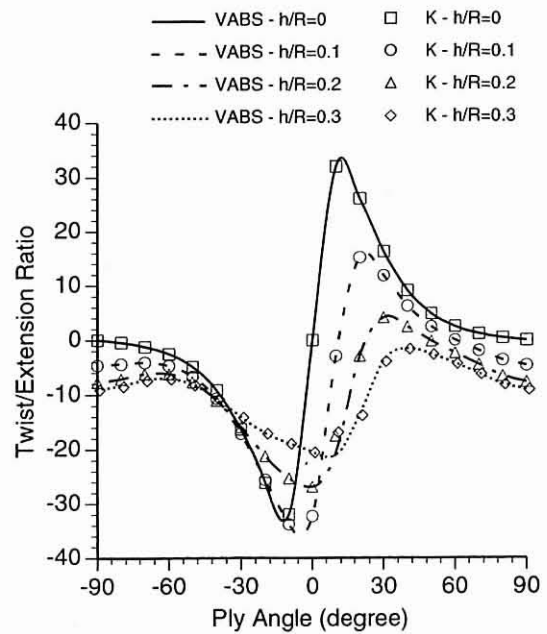


Fig. 14. Twist/extension ratio of APa for different levels of initial twist.

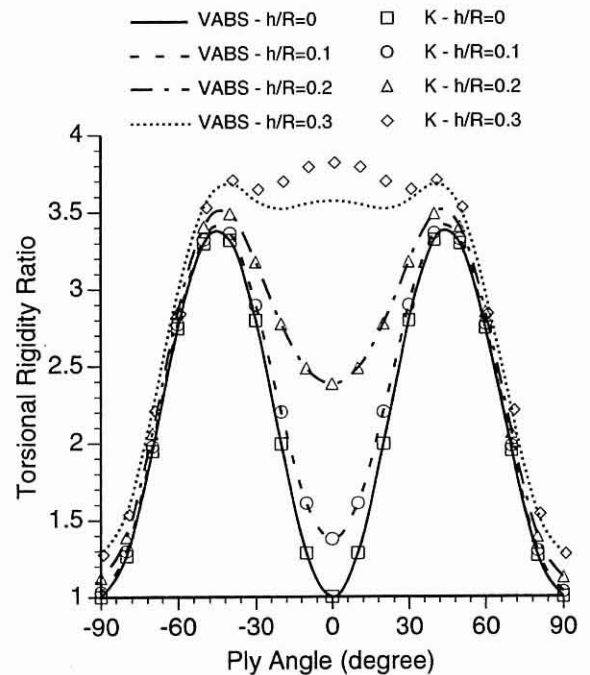


Fig. 15. Torsional rigidity ratio of APs for different levels of initial twist.

fidelity low-cost computational tool.

Concluding Remarks

A general framework for beam modeling is presented that allows an engineer to take advantage of composite materials when designing rotor blades. It is able to take into consideration anisotropic, nonhomogeneous materials and represent general cross-sectional geometries. The framework naturally leads to two separate analyses, one over the cross section

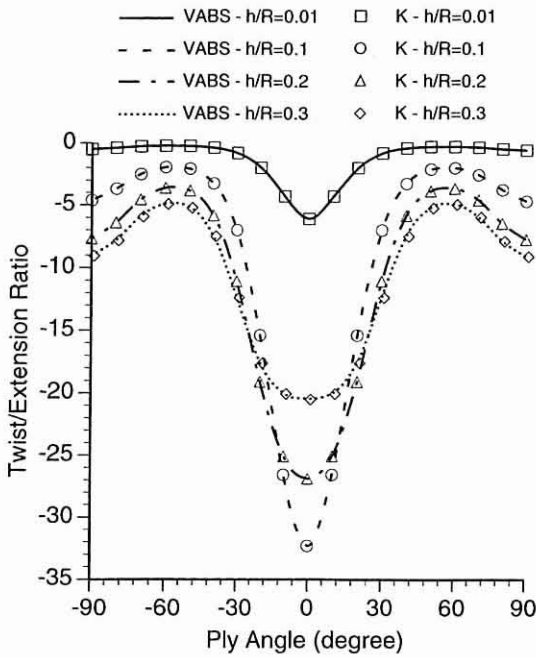


Fig. 16. Twist/extension ratio of APs for different levels of initial twist.

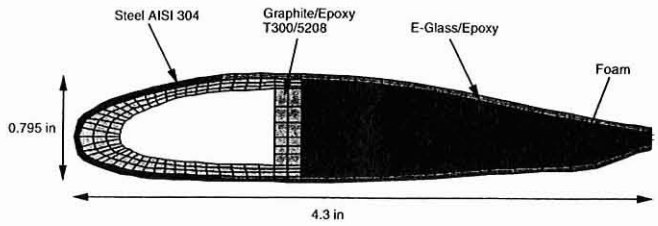


Fig. 18. Rotor blade (RB) test case.

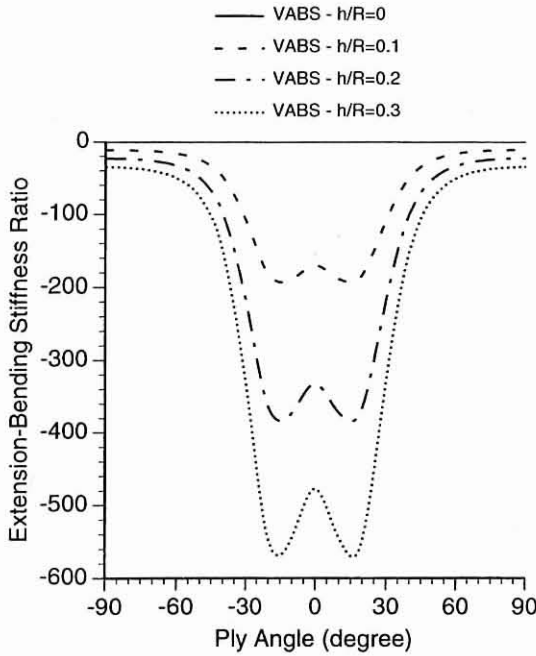


Fig. 17. Extension-bending coupling stiffness ratio of APs for different levels of initial curvature (k_3).

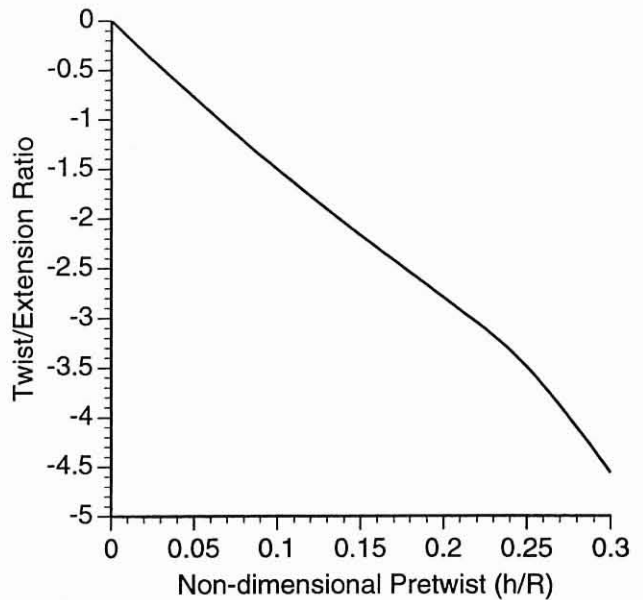


Fig. 19. Twist/extension ratio of the rotor blade (RB) for different levels of initial twist.

(VABS) and the other along the beam. (Note that VABS is derived from the same framework as the geometrically-exact mixed formulation for beam dynamics of Ref. 2.) Results obtained by using this framework are presented, and their accuracy indicates that this framework yields excellent predictive capability and, consequently, should lower costs from experimental tests and further adjustments. Thus, the designer does not need to bear either the cost of 3-D finite element discretization or the loss of accuracy inherent in any simplified representation of a blade cross section, such as a box beam. Although VABS is intended to be used along with a

geometrically-exact, mixed finite element formulation derived from the same framework, the 4×4 "classical" matrix can also be used with the non-linear beam element of 2GCHAS (Ref. 36). Finally, VABS is suitable for use as a tool in structural dynamics optimization procedures and aeroelastic tailoring.

VABS takes into account all possible deformation in the 3-D representation. Although it is a useful and powerful tool in its present form for analysis of composite rotor blades with arbitrary cross sections, the code still needs to be improved for certain non-classical refinements in the 1-D theory. For example, for bearingless rotor flexbeams (a beam with open section) one must account for restrained warping in the 1-D model, which may require the use of a rather complex procedure known as short-wavelength extrapolation. Here "non-classical" 1-D variables must be redefined

and incorporated into both the stiffness and dynamic models. A more engineering-oriented approach to this aspect of the problem is in progress under the sponsorship of the National Rotorcraft Technology Center.

Acknowledgements

This work was supported in part by the Center of Excellence for Rotorcraft Technology at the Georgia Institute of Technology, sponsored by the U.S. Army Research Office. The technical monitor is Dr. Gary L. Anderson.

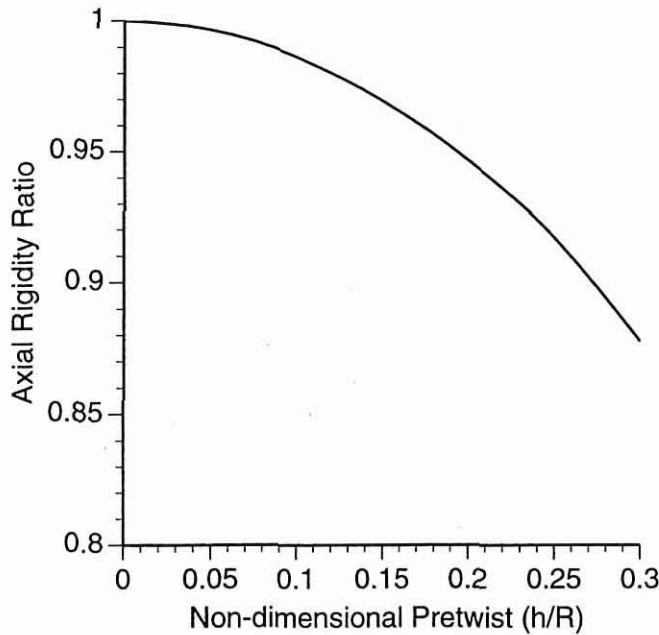


Fig. 20. Axial rigidity ratio of the rotor blade (RB) for different levels of initial twist.

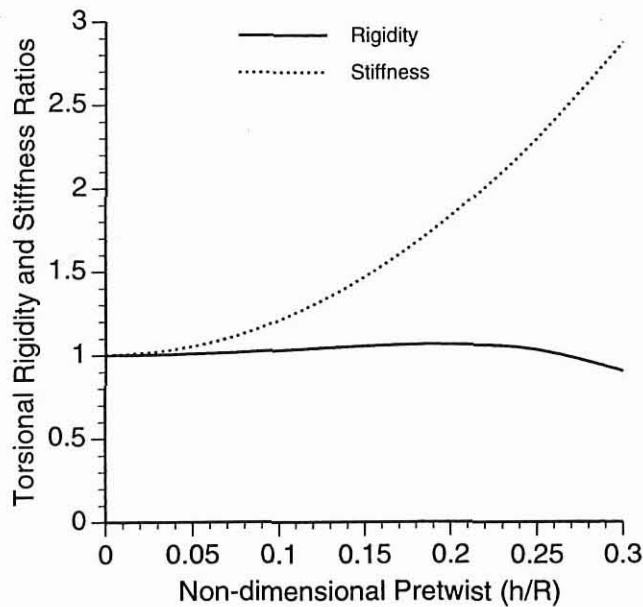


Fig. 21. Torsional rigidity and stiffness ratios of the rotor blade (RB) for different levels of initial twist.

References

¹Berdichevsky, V. L., "Variational-Asymptotic Method of Shell Theory Construction," *PMM*, Vol. 43, No. 4, 1979, pp. 664-687.
²Hodges, D. H., "A Mixed Variational Formulation Based on Exact Intrinsic Equations for Dynamics of Moving Beams," *International Journal of Solids and Structures*, Vol. 26, No. 11, 1990, pp. 1253-1273.
³Berdichevsky, V. L., "On the Energy of an Elastic Rod," *PMM*, Vol. 45, 1982, pp. 518-529.
⁴Hodges, D. H., Atilgan, A. R., Cesnik, C. E. S., and Fulton, M. V.,

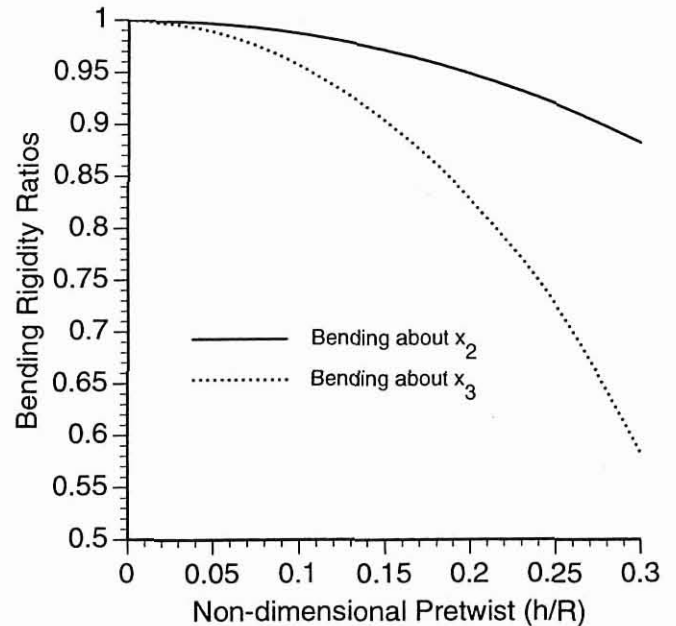


Fig. 22. Bending rigidity ratios of the rotor blade (RB) for different levels of initial twist.

"On a Simplified Strain Energy Function for Geometrically Nonlinear Behavior of Anisotropic Beams," *Composites Engineering*, Vol. 2, No. 5-7, 1992, pp. 513-526.

⁵Danielson, D. A. and Hodges, D. H., "Nonlinear Beam Kinematics by Decomposition of the Rotation Tensor," *Journal of Applied Mechanics*, Vol. 54, No. 2, 1987, pp. 258-262.

⁶Cesnik, C. E. S., Cross-Sectional Analysis of Initially Twisted and Curved Composite Beams, Ph.D. Thesis, Aerospace Engineering, Georgia Institute of Technology, May 1994.

⁷Cesnik, C. E. S., Sutyryn, V. G., and Hodges, D. H., "A Refined Composite Beam Theory Based on the Variational-Asymptotical Method," In *Proceedings of the 34th Structures, Structural Dynamics and Materials Conference*, La Jolla, California, Apr 19-22, 1993, pp. 2710-2720, AIAA Paper 93-1616.

⁸Cesnik, C. E. S., Sutyryn, V. G., and Hodges, D. H., "Refined Theory of Twisted and Curved Composite Beams: The Role of Short-Wavelength Extrapolation," *International Journal of Solids and Structures*, Vol. 33, No. 10, 1996, pp. 1387-1408.

⁹Sutyryn, V. G. and Hodges, D. H., "On Asymptotically Correct Plate Theory," In *Proceedings of the 36th Structures, Structural Dynamics and Materials Conference*, New Orleans, Louisiana, Apr 10-12, 1995, pp. 1800-1811, AIAA Paper 95-1373, to appear in the *International Journal of Solids and Structures*.

¹⁰Cesnik, C. E. S. and Hodges, D. H., "Stiffness Constants for Initially Twisted and Curved Composite Beams," *Applied Mechanics Reviews*, Vol. 46, No. 11, Part 2, 1993, pp. S211-S220.

¹¹Shang, X. and Hodges, D. H., "Aeroelastic Stability of Composite Hingeless Rotors with Advanced Configurations," In *Proceedings of the 37th Structures, Structural Dynamics and Materials Conference*, Salt Lake City, Utah, Apr 15-17, 1996, pp. 1991-2001, AIAA Paper 95-1548.

¹²Hodges, D. H., Shang, X., and Cesnik, C. E. S., "Finite Element Solution of Nonlinear Intrinsic Equations for Curved Composite Beams," *Journal of the American Helicopter Society*, Vol. 41, No. 4, 1996, pp.313-321.

¹³Bathe, K., *Finite Element Procedures in Engineering Analysis*, Prentice-Hall, Englewood Cliffs, NJ, 1982.

¹⁴Anon., *I-DEAS™ Finite Element Modeling User's Guide for the Integrated Design Engineering Analysis Software (SDRC I-DEAS)*, Structural Dynamics Research Corporation, Milford, Ohio, 1990.

¹⁵Collins, R. J., "Bandwidth Reduction by Automatic Renumbering," *International Journal for Numerical Methods in Engineering*, Vol. 6, 1973, pp. 345-356.

¹⁶Anon., *MSC/NASTRAN User's Guide*, The MacNeal-Schwendler Corporation, Los Angeles, California, 1985.

¹⁷Gibson, W. C. and Parekh, J. C., *Variation-Asymptotic Beam Analysis Software for Rotor Blades*, CSA Engineering, Inc., Palo Alto, California, December 1994.

¹⁸Lanczos, C., "An Iteration Method for the Solution of the Eigenvalue Problem of Linear Differential and Integral Operators," *Journal of Research of the National Bureau of Standards*, Vol. 45, No. 4, 1950, pp. 255-282.

¹⁹Jones, M. T. and Patrick, M. L., "LANZ — Software for Solving the Large Sparse Symmetric Generalized Eigenproblem," Technical Report Program No. LAR-14506, Cosmic, Athens, Georgia, 1990.

²⁰Nour-Omid, B., Parlett, B. N., and Taylor, R. L., "Lanczos versus Subspace Iteration for Solution of Eigenvalue Problems," *International Journal for Numerical Methods in Engineering*, Vol. 19, 1983, pp. 859-871.

²¹Jones, M. T. and Patrick, M. L., "The Use of Lanczos Method to Solve the Large Generalized Symmetric Definite Eigenvalue Problem," Technical report 89-69, Institute for Computer Applications in Science and Engineering (ICASE), 1989.

²²Minguet, P. and Dugundji, J., "Experiments and Analysis for Composite Blades Under Large Deflections, Part I — Static Behavior," *AIAA Journal*, Vol. 28, No. 9, Sep 1990, pp. 1573-1579.

²³Giavotto, V., Borri, M., Mantegazza, P., Ghiringhelli, G., Carmaschi, V., and Maffioli, G. C., "Anisotropic Beam Theory and Applications," *Computers and Structures*, Vol. 16, No. 1-4, 1983, pp. 403-413.

²⁴Stemple, A. D. and Lee, S. W., "Finite Element Model for Composite Beams with Arbitrary Cross Sectional Warping," *AIAA Journal*, Vol. 26, No. 12, 1988, pp. 1512-1520.

²⁵Hodges, D. H., Atilgan, A. R., Fulton, M. V., and Rehfield, L. W., "Free-Vibration Analysis of Composite Beams," *Journal of the American Helicopter Society*, Vol. 36, No. 3, 1991, pp. 36-47.

²⁶Berdichevsky, V. L., Armanios, E. A., and Badir, A. M., "Theory of Anisotropic Thin-Walled Closed-Section Beams," *Composites Engineering*, Vol. 2, No. 5-7, 1992, pp. 411-432.

²⁷Hodges, R. V., Nixon, M. W., and Rehfield, L. W., "Comparison of Composite Rotor Blade Models: A Coupled-Beam Analysis and an MSC/NASTRAN Finite-Element Model," Technical Memorandum 89024, NASA, March 1987.

²⁸Chandra, R., Stemple, A. D., and Chopra, I., "Thin-Walled Composite Beams Under Bending, Torsional, and Extensional Loads," *Journal of Aircraft*, Vol. 27, No. 7, 1990, pp. 619-626.

²⁹Smith, E. C. and Chopra, I., "Formulation and Evaluation of an Analytical Model for Composite Box-Beams," In *Proceedings of the 31st Structures, Structural Dynamics and Materials Conference*, Apr 2-4, 1990, pp. 759-783, AIAA Paper 90-0962.

³⁰Rehfield, L. W. and Atilgan, A. R., "Shear Center and Elastic Axis and their Usefulness for Composite Thin-Walled Beams," In *Proceedings of the American Society for Composites, Fourth Technical Conference*, Blacksburg, Virginia, 1989, pp. 179-188.

³¹Chandra, R. and Chopra, I., "Structural Response of Composite Beams and Blades with Elastic Couplings," *Composites Engineering*, Vol. 2, No. 5-7, 1992, pp. 347-374.

³²Vlasov, V. Z., *Thin-Walled Elastic Beams*, National Science Foundation and Department of Commerce, 1961.

³³Badir, A. M., Berdichevsky, V. L., and Armanios, E. A., "Theory of Composite Thin-Walled Opened Cross Section Beams," In *Proceedings, 34th Structures, Structural Dynamics, and Materials Conference*, La Jolla, California, Apr 1993, pp. 2761-2770.

³⁴Kosmatka, J. B., "Extension-Bend-Twist Coupling Behavior of Thin-Walled Advanced Composite Beams with Initial Twist," In *Proceedings of the 32nd Structures, Structural Dynamics, and Materials Conference*, Baltimore, Maryland, Apr 8-10, 1991, pp. 1037-1049, AIAA Paper 91-1023.

³⁵Cesnik, C. E. S., Hodges, D. H., and Sutyryn, V. G., "Stiffness Constants for Composite Beams Including Large Initial Twist and Curvature Effects," *AIAA Journal*, Vol. 14, No. 9, 1996, pp. 1913-1920.

³⁶Anon., "2GCHAS Theory Manual," USAATCOM Technical Memorandum 93-A-004, U.S. Army Aviation and Troop Command, Moffett Field, California, 1993.